ACS APPLIED POLYMER MATERIALS

pubs.acs.org/acsapm
Article

Bespoke Block Copolymer Nanoparticles Boost the Thermal Conductivity of Oils

Priyanka Chohan, Oleksandr O. Mykhaylyk, Steven P. Armes,* Giles M. Prentice, and David J. Atkinson

Cite This: https://doi.org/10.1021/acsapm.6c03043

ABSTRACT: Next-generation thermal management fluids are urgently required for the efficient cooling of data centers and fast-charging batteries. To address this problem, we have prepared diblock copolymer nanoparticles with polar cores in non-polar media using polymerization-induced self-assembly (PISA). This is achieved via reversible addition−fragmentation chain transfer (RAFT) dispersion polymerization of 2-hydroxyethyl methacrylate (HEMA) using an oil-soluble poly(lauryl methacrylate) (PLMA) precursor in a poly(α-olefin) oil. This synthetic protocol affords a low-viscosity dispersion of PLMA−PHEMA nanoparticles of approximately 100 nm diameter at up to 30% w/w solids. The PHEMA cores of such nanoparticles can be swollen with aqueous acid without any loss of colloidal stability, as judged by dynamic light scattering. Such acid-swollen nanoparticles serve as nanoreactors for the *in situ* synthesis of silica using an oil-soluble precursor (tetraethyl orthosilicate, TEOS). Thermogravimetric analysis reveals that the resulting nanocomposite nanoparticles contain up to 27% silica by mass. Extensive thermal conductivity measurements have been performed as a function of copolymer concentration, aqueous acid content, and temperature on the as-prepared PLMA−PHEMA nanoparticle dispersions, the acid-swollen nanoparticles, and the silica-loaded nanoparticles. The as-prepared nanoparticles boost thermal conductivity by up to 6.0%, with minimal increase in the kinematic viscosity of the dispersion. The addition of aqueous acid and the *in situ* formation of silica within the nanoparticle cores lead to further enhancements in thermal conductivity. Interestingly, colloidal dispersions of the silica-loaded nanocomposite nanoparticles can be engineered to be highly transparent at a given temperature, which could be an important advantage for their potential use as a next-generation thermal management fluid.

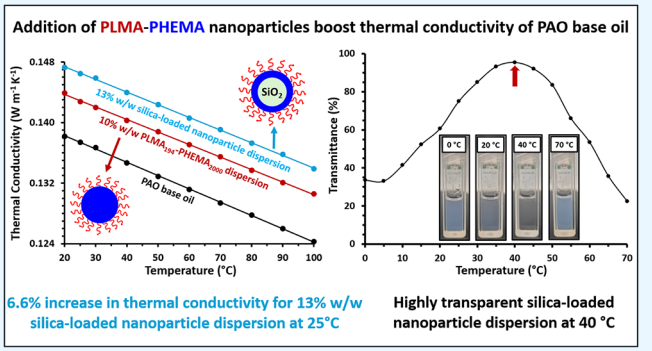

KEYWORDS: *RAFT polymerization, block copolymer nanoparticles, thermal management fluids, polymerization-induced self-assembly, polymer−silica nanocomposites, nonpolar media*

INTRODUCTION

World Wide Web (WWW) data storage centers and the rapid recharging of electric car batteries both require low-viscosity liquid coolants that combine high thermal conductivity with very low electrical conductivity.[1−5] In principle, continuous recirculation of such thermal management fluids should ensure efficient heat dissipation and prevent chemical degradation caused by localized overheating. The global market for thermal management fluids is predicted to be worth $5.8 billion by 2027.[6] In principle, water could be used as a thermal management fluid: it has a high thermal conductivity (0.60 W m^{-1} K^{-1})[7] and is nonflammable, nontoxic and cost-effective. Unfortunately, its electrical conductivity is far too high for this application. In contrast, oils have very low electrical conductivity but suffer from relatively low thermal conductivity (~0.13 W m^{-1} K^{-1}).[8] According to the literature, oil thermal conductivity can be boosted by introducing various types of inorganic nanoparticles such as silica or alumina but the resulting slurries often suffer from poor colloidal stability.[5,9−14] This produces viscous suspensions that prevent energy-efficient continuous recirculation, which is a prerequisite for effective heat dissipation.

Polymerization-induced self-assembly (PISA) involves growing an insoluble (B) block from one end of a soluble (A) precursor block in a suitable solvent: *in situ* self-assembly occurs at some critical degree of polymerization (DP) of the B block to produce sterically stabilized diblock copolymer nanoparticles (see Scheme 1). Importantly, PISA works extremely well in non-polar media.[15−30] This versatile platform technology enables the efficient synthesis of well-defined spherical nanoparticles directly in non-polar solvents (e.g., *n*-

Received: July 11, 2026
Revised: August 18, 2026
Accepted: August 19, 2026

Scheme 1. Schematic Synthesis of the $PLMA_{194}$−$PHEMA_{2000}$ Nanoparticles and the Corresponding Silica-Loaded Nanoparticles Examined in this Study

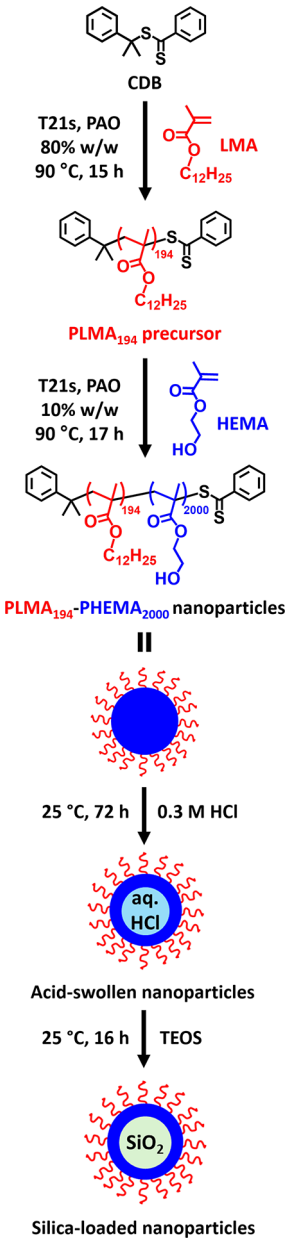

dodecane, mineral oil, or poly(α-olefins) (PAOs)).[19,31,32] Such dispersions exhibit excellent long-term colloidal stability and minimal viscosity. Potential applications for such nanoparticles include lubricating additives for automotive engine oils.[22,24,29]

Recently, we reported the preparation of well-defined block copolymer nanoparticles by conducting the reversible addition−fragmentation chain transfer (RAFT)[33,34] dispersion polymerization of 2-hydroxyethyl methacrylate (HEMA) in *n*-dodecane at 90 °C using poly(lauryl methacrylate) (PLMA) as an oil-soluble precursor.[32] Well-defined spherical nanoparticles with PHEMA cores were obtained when targeting PHEMA DPs of up to 1000. A monomer-starved feed protocol afforded relatively narrow, unimodal particle size distributions; in contrast, a one-shot batch protocol invariably produced bimodal particle size distributions when targeting higher PHEMA DPs owing to a side-reaction between the HEMA monomer and the dithiobenzoate-capped chains.

Herein we revisit the PISA syntheses of such PLMA−PHEMA nanoparticles to evaluate them as an additive for the design of next-generation thermal management fluids. In principle, the highly polar nature of the PHEMA cores should boost the thermal conductivity of such colloidal dispersions above that of the base oil.[35] Accordingly, we perform PISA syntheses of $PLMA_{194}$−$PHEMA_{2000}$ nanoparticles in a suitable poly(α-olefin), rather than *n*-dodecane (see Scheme 1). Highly polar monomers such as HEMA typically exhibit fast kinetics when polymerized under heterogeneous conditions in non-polar media.[31,32] Nevertheless, incomplete monomer conversions are inevitably observed in the high DP limit.[25] In the present study, this problem has been offset by conducting PISA syntheses at up to 30% w/w solids, which also makes such syntheses more process-intensive. We examine the use of PLMA−PHEMA nanoparticles as nanoreactors for the *in situ* synthesis of silica within their cores without any loss in colloidal stability using tetraethyl orthosilicate (TEOS) as an oil-soluble silica precursor, see Scheme 1. In principle, such nanocomposite nanoparticles should further enhance the thermal conductivity of the oil phase without producing a highly viscous fluid. Finally, we also demonstrate the feasibility of preparing *highly transparent* dispersions: in principle, this should allow visual inspection of electrical circuitry for signs of long-term corrosion without having to drain the thermal management fluid from the enclosed system.

EXPERIMENTAL SECTION

Materials

Lauryl methacrylate (LMA; 96%) was purchased from Sigma-Aldrich (UK) and filtered through basic alumina to remove monomethyl ether hydroquinone (MEHQ) inhibitor prior to use. 2-Hydroxyethyl methacrylate (HEMA, triply distilled ULTRA grade; 0.1 mol % dimethacrylate impurity) was kindly provided by GEO Specialty Chemicals (Hythe, UK) and was used as received. Cumyl dithiobenzoate (CDB; 99%), tetraethyl orthosilicate (TEOS; 98%), 2,6-di-*tert*-butyl-4-methyl-phenol (BHT; 99%), ruthenium(IV) oxide hydrate and sodium periodate (99.8%) were purchased from Sigma-Aldrich (UK). Hydrochloric acid (HCl; 37%), *n*-dodecane and d_5-pyridine were purchased from Thermo Fisher Scientific (UK). d_2-Dichloromethane (CD_2Cl_2) was purchased from Cambridge Isotope Laboratory (USA). Tetrahydrofuran (THF; HPLC grade) and triethylamine (TEA; 99%) were obtained from VWR Chemicals (UK) and *tert*-butyl peroxy-2-ethylhexanoate (T21s) initiator was supplied by AkzoNobel (The Netherlands). The poly(α-olefin) oil (PAO; Durasyn 162) was provided by Castrol Ltd. (Pangbourne, UK) and *n*-heptane was purchased from Alfa Aesar (UK). Deionized water (resistivity = 15 MΩ·cm) was obtained from an Elgastat Option 3A water purification system.

Synthesis of Block Copolymer Nanoparticles via RAFT Dispersion Polymerization of HEMA

The $PLMA_{194}$−$PHEMA_{2000}$ nanoparticles were prepared as follows. First a $PLMA_{194}$ homopolymer was prepared at 80% w/w solids by adapting a previously reported protocol.[19] LMA (59.77 g; 0.235 mol), CDB (0.32 g; 1.175 mmol; target DP = 200), T21s initiator (84.7 mg; 0.392 mmol; CDB/T21s molar ratio = 3.0; dissolved at 10% v/v in 0.678 g PAO) and PAO (14.36 g) were weighed into a 100 mL round-bottomed flask containing a magnetic flea, which was sealed using a rubber septum. The resulting solution was purged with nitrogen gas for 30 min. Then the sealed flask was immersed in a preheated oil bath at 90 °C to initiate the LMA polymerization and the reaction mixture was magnetically stirred for 15 h. A final LMA conversion of 97% was determined by ^{1}H NMR spectroscopy studies

https://doi.org/10.1021/acsapm.6c03043
ACS Appl. Polym. Mater. XXXX, XXX, XXX−XXX

in CD_2Cl_2 by comparing the integrated vinyl monomer signals at 5.6 and 6.1 ppm to the two oxymethylene protons assigned to PLMA at 3.8−4.1 ppm. Accordingly, the mean DP of this crude PLMA precursor was calculated to be approximately 194. THF GPC analysis using a refractive index detector and a series of near-monodisperse poly(methyl methacrylate) calibration standards indicated an M_n of 40 100 g mol^{-1} and an M_w/M_n of 1.16. This $PLMA_{194}$ precursor was then chain-extended to prepare $PLMA_{194}$−$PHEMA_{2000}$ nanoparticles at 10% w/w solids *via* monomer-starved addition of HEMA, as previously reported.[32] The synthesis of the $PLMA_{194}$−$PHEMA_{2000}$ nanoparticles was conducted as follows. The as-synthesized $PLMA_{194}$ precursor (4.000 g, 80% w/w solids; 64.5 μmol), T21s initiator (4.65 mg; 21.5 μmol; dissolved at 10% v/v in 0.0372 g PAO) and PAO (179.09 g) were weighed into a 500 mL round-bottomed flask equipped with a magnetic flea. HEMA monomer (18.0 g) was added to a separate 14 mL glass vial. Both vials were then sealed and purged with nitrogen gas for 30 min. Degassed HEMA monomer (16.78 g; 129.0 mmol; target DP = 2000) was drawn into a degassed 24 mL syringe, which was then placed into a motorized Aladdin AL-1000 syringe pump. The flask containing the $PLMA_{194}$ precursor was immersed in a preheated oil bath set at 90 °C, and HEMA monomer was added dropwise over 2.0 h at a rate of 7.82 mL h^{-1} with continuous magnetic stirring. After complete addition of this monomer, the polymerization was allowed to proceed for a further 15 h at 90 °C. A final HEMA conversion of more than 99% (i.e., no detectable monomer vinyl signals) was determined *via* ^{1}H NMR analysis in d_5-pyridine, indicating a PHEMA DP of approximately 2000. This protocol can also be used to prepare well-defined $PLMA_{194}$−$PHEMA_{2000}$ nanoparticles of approximately 100 nm diameter at either 20% or 30% w/w solids in PAO (>99% HEMA conversion): see Table S1 for a summary of all the reagent and solvent masses used to prepare the diblock copolymers. However, targeting 40% w/w solids led to the formation of larger, more polydisperse nanoparticles (see Table S2 and Figure S1).

Synthesis of Silica-Loaded Block Copolymer Nanoparticles

Before preparation of the silica-loaded nanoparticles, the nanoparticles were swollen using aqueous acid. A 10% w/w dispersion of $PLMA_{194}$−$PHEMA_{2000}$ nanoparticles prepared under monomer-starved conditions in PAO (35.0 g; corresponding to 2.939 g $PHEMA_{2000}$) and an aqueous solution of 0.3 M HCl (0.8817 g, 30% w/w based on the $PHEMA_{2000}$ mass; 48.9 mmol water) were placed in a 60 mL glass jar, sealed and stirred at 1000 rpm for 3 days at 25 °C to obtain the acid-swollen $PLMA_{194}$−$PHEMA_{2000}$ nanoparticles. TEOS (2.5489 g; 12.23 mmol) was then added *via* micropipette to the jar, which was shaken for 30 s before allowing to stand unstirred for 16 h at 25 °C. This process was repeated to produce nanoparticles with a higher silica loading by increasing the mass of TEOS (4.5880 g; 22.02 mmol). Finally, ethanol and water were removed from the cores of the final nanoparticles by annealing portions of such colloidal dispersions at 95 °C for 2 h.

Preparation of Dried Silica-Loaded $PLMA_{194}$−$PHEMA_{2000}$ Nanoparticles

The silica-loaded nanoparticles were purified by centrifugation and dried to enable quantitative determination of their silica content by thermogravimetric analysis (TGA). First, 11−12% w/w dispersions of silica-loaded nanoparticles dispersed in PAO (0.80 g) were placed in 1.5 mL microfuge tubes. Pairs of tubes were mass-balanced before being placed in a microcentrifuge (Heraeus Biofuge Pico D-37520) and centrifugation was conducted for 60 min at 13,000 rpm. The supernatant was decanted and the sedimented nanoparticles were redispersed in *n*-heptane (0.50 mL) prior to centrifugation for 20 min at 13,000 rpm. This centrifugation-redispersion was repeated and the moist nanoparticle sediments were placed in a vacuum oven and dried at 40 °C for 3 days. The original (non-swollen) $PLMA_{194}$−$PHEMA_{2000}$ nanoparticles were also dried following the same protocol.

CHARACTERIZATION TECHNIQUES

^{1}H NMR Spectroscopy

^{1}H NMR spectra were recorded at 298 K in either CD_2Cl_2 or d_5-pyridine using a 400 MHz Bruker Avance spectrometer. Typically, 64 scans were averaged per spectrum.

Gel Permeation Chromatography (GPC)

THF GPC was used to assess the molecular weight distribution (MWD) of the $PLMA_{194}$ precursor. The instrument comprised an Agilent 1260 GPC system and two Agilent PL gel 5 μm Mixed C columns, which were connected in series with a guard column and a 1260 Infinity II refractive index detector. The eluent contained BHT (1.25 g) and TEA (50 mL) in HPLC-grade THF (2500 mL), the operating temperature was 30 °C and the flow rate was 1.0 mL min^{-1}. A series of nine near-monodisperse poly(methyl methacrylate) standards (with M_p values ranging from 7,290 to 2,210,000 g mol^{-1}) were used for calibration.

Dynamic Light Scattering (DLS)

DLS studies were conducted using a Zetasizer Nano ZS instrument (Malvern Instruments, UK) at a fixed scattering angle of 173°. The copolymer dispersions were diluted to 0.10% w/w using *n*-dodecane prior to light scattering studies at 25 °C. DLS was also used to assess the thermal stability of the as-prepared $PLMA_{194}$−$PHEMA_{2000}$ nanoparticles and 26.7% silica-loaded nanoparticles between 20 and 80 °C. The z-average hydrodynamic diameter and DLS polydispersity were calculated by cumulant analysis of the experimental correlation function using Dispersion Technology Software version 6.20 and assuming that the Stokes−Einstein equation is valid. Data were averaged over three consecutive runs comprising ten measurements per run.

Transmission Electron Microscopy (TEM)

TEM images were recorded using a JEOL JEM-120i electron microscope operating at 120 kV and equipped with a SightSKY 19 megapixel camera. A single droplet of a 0.10% w/w copolymer dispersion diluted in *n*-dodecane was placed on a carbon-coated copper grid and air-dried for 90 min prior to exposure to ruthenium(VIII) oxide vapor for 7 min at 20 °C.[36] This heavy metal compound acted as a positive stain to improve electron contrast and was prepared as follows. Ruthenium(IV) oxide (0.30 g) was added to water (50 g) to form a black slurry; addition of sodium periodate (2.0 g) with continuous stirring produced a yellow solution of ruthenium(VIII) oxide within 1 min at 20 °C. Analytical X-ray mapping images were recorded using a JEOL JEM-F200 field emission analytical scanning transmission electron microscope operating at 200 kV equipped with an energy dispersive X-ray detector.

Thermogravimetric Analysis (TGA)

Mass loss curves were recorded for the dried precursor $PLMA_{194}$−$PHEMA_{2000}$ nanoparticles and the silica-loaded $PLMA_{194}$−$PHEMA_{2000}$ nanoparticles using a Q500 TA TGA instrument. Samples were heated under air from 20 to 800 °C at a heating rate of 10 °C min^{-1}.

Thermal Conductivity Measurements

Thermal conductivities of the nanoparticle dispersions were determined using a Flucon LAMBDA Thermal Conductivity Meter equipped with a TECHNE UCAL 400+ dry block thermostat. The sensor cell was filled in turn with 35 mL of each dispersion and subsequently placed in the dry block thermostat. A series of ten measurements (each of 30 s

https://doi.org/10.1021/acsapm.6c03043
ACS Appl. Polym. Mater. XXXX, XXX, XXX−XXX

duration) was recorded at 25 °C. The discrete temperature setting was employed for measurements made between 20 and 100 °C, whereby ten measurements were recorded at each 10 °C interval. Data were acquired with a precision of ±1% using FluconLAM software (version 8).

Dielectric Constant Measurements

Dielectric constants of the nanoparticle dispersions were determined with a Flucon EPSILON+ dielectricity meter using the international standard for measuring the dielectric properties of liquid electrical insulators (DIN IEC 60247). The cell was filled with each nanoparticle dispersion (8.0 mL) before being placed within the instrument and heated to 30 °C. A series of measurements were recorded and an average value was calculated.

Rotational Rheology

An Anton Paar MCR 502 rheometer, with a TruGap functionality for online monitoring of the geometry gap, a variable-temperature Peltier plate, Peltier hood and a 50 mm 2° measuring cone was used for all rheology measurements. The dynamic viscosity of each as-prepared, acid-swollen or silica-loaded $PLMA_{194}$−$PHEMA_{2000}$ nanoparticle dispersion (approximately 1.5 mL) was determined as a function of shear rate (1−1000 s^{-1}) at 25 °C with a zero-gap set at 207 μm. Dynamic viscosity measurements were also performed at shear rates of 1−1000 s^{-1} at 40, 55, or 70 °C on both the PAO oil and the as-prepared 10% w/w $PLMA_{194}$−$PHEMA_{2000}$ nanoparticle dispersion.

Solution Densitometry

Solution densities (± 0.000005 g cm^{-3}) were determined using an Anton Paar DMA 5000 densitometer operating at 25 to 70 °C. Known concentrations of the as-prepared, acid-swollen or silica-loaded $PLMA_{194}$−$PHEMA_{2000}$ nanoparticle dispersions (1.0 mL) were prepared before being injected in turn into a U-shaped borosilicate glass tube. After allowing 5 min for temperature equilibration, the solution density (ρ) of each dispersion was determined. Given the dynamic viscosity (μ) of the corresponding sample (obtained by rotational rheology), such densities were used to determine the kinematic viscosity (ν) using the equation $\nu = \frac{\mu}{\rho}$.

Small-Angle X-ray Scattering (SAXS)

SAXS experiments were conducted at station ID02 of the European Synchrotron Radiation Facility (Grenoble, France) using monochromatic X-ray radiation (λ = 0.103 nm) and an Eiger2 4M two-dimensional detector (Dectris, Switzerland). The measurements covered a q range of 0.04−3.6 nm^{-1}, where q is the magnitude of the scattering vector, defined as $q = 4\pi\sin\theta/\lambda$, with θ denoting half of the scattering angle. The samples comprised dispersions of $PLMA_{194}$−$PHEMA_{2000}$ nanoparticles in PAO, acid-swollen $PLMA_{194}$−$PHEMA_{2000}$ nanoparticles in PAO (using a 30% w/w aqueous solution of 0.3 M HCl based on the PHEMA mass) and silica-loaded $PLMA_{194}$−$PHEMA_{2000}$ nanoparticles in PAO. A flow-through glass capillary of 1.58 mm diameter was used as a sample holder. Scattering data (including a correction for secondary scattering contributions from the beamline windows)[37] were reduced using standard routines provided by the beamline and were further analyzed using Irena SAS macro for Igor Pro.[38]

UV−Visible Absorption Spectroscopy

UV−visible spectra were recorded in transmittance mode using an Agilent Cary 3500 Multicell UV−visible spectrophotometer equipped with a 250 Hz xenon flash lamp and Agilent Cary UV workstation 1.3.4 software. Spectra for the silica-loaded $PLMA_{194}$−$PHEMA_{2000}$ nanoparticles were recorded at 400 nm between 0 and 70 °C, with measurements taken at 5 °C intervals using a Multicell Peltier UV−visible detector module with an averaging time of 0.100 s and a spectral bandwidth of 2 nm. Prior to each measurement, a baseline spectrum for the PAO was recorded at each temperature.

RESULTS AND DISCUSSION

In principle, the synthesis of the target $PLMA_{200}$−$PHEMA_x$ diblock copolymer nanoparticles via RAFT dispersion polymerization outlined in Scheme 1 can be conducted using either a dithiobenzoate RAFT agent or a trithiocarbonate RAFT agent. However, an important constraint for commercially viable thermal management fluids is that their sulfur content should be minimized to avoid corrosion.[39] According to the industrial sponsor of this project (Castrol Ltd.), end users prefer a sulfur level of no more than 25 ppm for such applications. Clearly, this is a potential problem if such nanoparticles are to be prepared by RAFT polymerization owing to the organosulfur-based chain-ends. Thus we targeted relatively high PHEMA DPs (≥1,000) to minimize the overall sulfur content of the final nanoparticle dispersion. Inspecting Figure 1 in this context provides some useful insights regarding the theoretical sulfur content of such dispersions. For example, targeting $PLMA_{200}$−$PHEMA_{2000}$ nanoparticles at 10% w/w solids when using a cumyl dithiobenzoate RAFT agent allows the overall sulfur content of the dispersion to remain below 25 ppm. In principle, targeting $PLMA_{200}$−$PHEMA_{3000}$ nanoparticles at either 10% or 15% w/w solids also enables this stringent criterion to be fulfilled. On the other hand, the only formulation that allows a sulfur content of less than 25 ppm to be achieved when using a trithiocarbonate-based RAFT agent requires $PLMA_{200}$−$PHEMA_{3000}$ nanoparticles to be targeted at 10% w/w solids. Unfortunately, in our experience such PISA syntheses begin to become irreproducible when targeting PHEMA DPs at or above 3,000, with incomplete HEMA conversions sometimes being observed owing to the relatively low initiator concentration. In summary, using a dithiobenzoate RAFT agent for such nanoparticle syntheses offers a decisive advantage over the analogous trithiocarbonate RAFT agent if reproducible syntheses are required when targeting sulfur contents below 25 ppm. In view of these calculations, the reaction conditions employed in this study are exclusively focused on the synthesis of $PLMA_{200}$−$PHEMA_{2000}$ nanoparticles using a dithiobenzoate RAFT agent at 10−30% w/w solids, with the higher concentrations being explored simply for the purpose of demonstrating process intensification; all thermal conductivity measurements were conducted at 10−15% w/w solids (or lower).

Characterization of the As-Prepared $PLMA_{194}$−$PHEMA_{2000}$ Nanoparticles

GPC analysis of the $PLMA_{194}$ precursor indicated an apparent M_n of 40,100 g mol^{-1} and an M_w/M_n of 1.16, indicating good RAFT control. Unfortunately, it was not possible to perform GPC analysis of the final $PLMA_{194}$−$PHEMA_{2000}$ diblock copolymer since it proved to be insoluble in DMF. This is attributed to the presence of 0.1 mol % dimethacrylate within the HEMA monomer, which inevitably leads to crosslinking when targeting such a high degree of polymerization for the PHEMA block.[32,40,41]

https://doi.org/10.1021/acsapm.6c03043
ACS Appl. Polym. Mater. XXXX, XXX, XXX−XXX

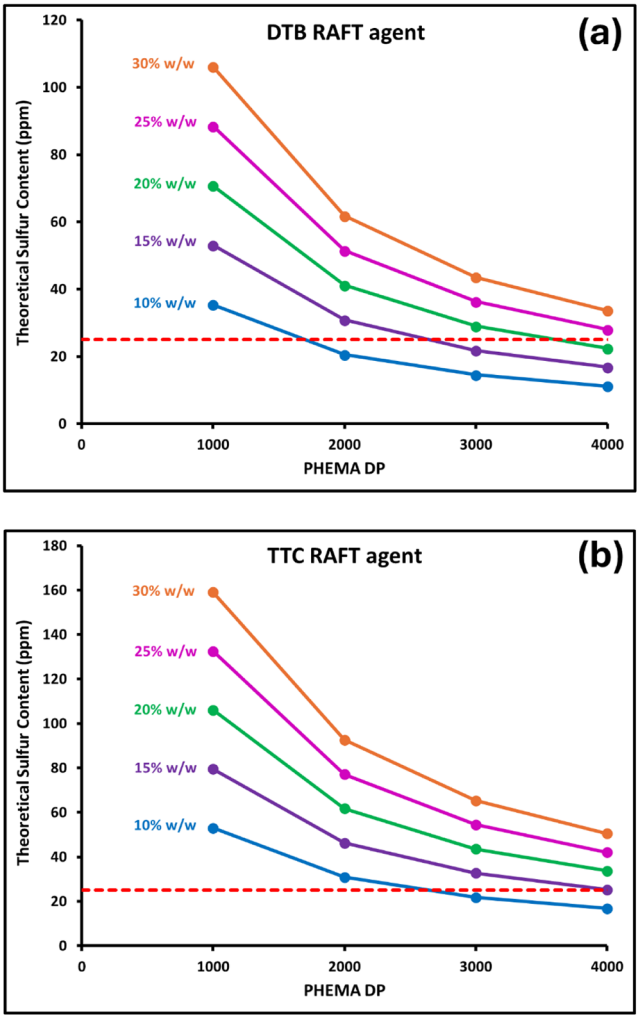

Figure 1. Theoretical sulfur content (ppm) calculated for colloidal dispersions of poly(lauryl methacrylate)-poly(2-hydroxyethyl methacrylate) ($PLMA_{200}$–$PHEMA_x$) nanoparticles prepared in a poly(α-olefin) oil at various copolymer concentrations when targeting a given PHEMA DP (or x): (a) using a dithiobenzoate (DTB) RAFT agent; (b) using a trithiocarbonate (TTC) RAFT agent. In each case, the PLMA stabilizer block has a fixed DP of 200 and the horizontal red line indicates the maximum permissible sulfur content of 25 ppm for a commercially viable thermal management fluid.

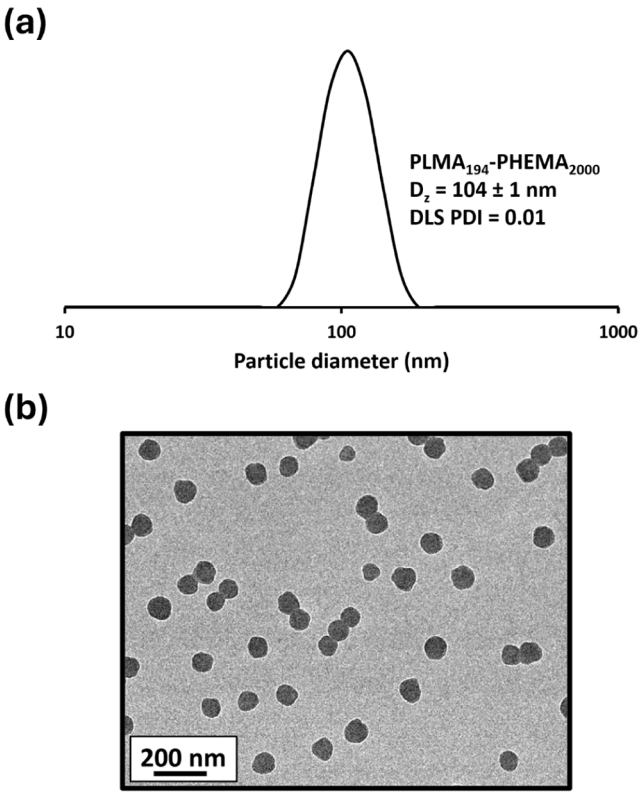

Figure 2. (a) DLS particle size distribution recorded for a 0.1% w/w dispersion of $PLMA_{194}$–$PHEMA_{2000}$ nanoparticles. (b) Representative TEM image recorded for the same nanoparticles.

Excellent reproducibility was observed for such RAFT dispersion polymerizations, with ^{1}H NMR spectroscopy studies invariably confirming a final HEMA conversion of more than 99%. Similarly, DLS studies indicated a hydrodynamic z-average diameter of 104 nm for the final sterically stabilized diblock copolymer nanoparticles, which possess a pseudo-spherical morphology and a relatively narrow particle size distribution as judged by TEM studies (see Figure 2).

Thermal Conductivity Measurements: Effect of Copolymer Concentration and Temperature

Thermal conductivity data obtained for varying concentrations of $PLMA_{194}$–$PHEMA_{2000}$ nanoparticles in PAO at 25 °C are shown in Figure 3a and Table S3 (see Supporting Information). A linear relationship is observed and the thermal conductivity of a 10% w/w nanoparticle dispersion is approximately 3.9% higher than that of PAO alone. This enhancement is attributed to the highly polar nature of the PHEMA nanoparticle cores. In principle, this means that such nanoparticle dispersions should be more effective thermal management fluids than the PAO alone. On the other hand, the presence of 10% w/w nanoparticles leads to a 25% increase in the kinematic viscosity at the same temperature. Given that it requires more energy to circulate a more viscous thermal management fluid, there is clearly a trade-off in overall performance. Heating above 25 °C leads to a significant reduction in viscosity, as expected (see Table S4, Figure S3 and Figure S4). For example, the dynamic viscosity of the nanoparticle dispersion is reduced by 75% when heating up to 70 °C, while that for the PAO oil alone is reduced by 86% at the same temperature. Moreover, the dynamic viscosity is essentially independent of the applied shear rate from around 10–50 s^{-1} up to 1000 s^{-1}, indicating Newtonian behavior under such conditions.

To target the highest possible thermal conductivity enhancement while remaining below the upper limit sulfur content of 25 ppm (see Figure 1a), we also targeted $PLMA_{194}$–$PHEMA_{2600}$ nanoparticles at 15% w/w solids with HEMA monomer addition over 2.6 h. ^{1}H NMR spectroscopy studies indicated a final HEMA conversion of 99% after 15 h at 90 °C while DLS analysis reported a z-average diameter of 119 nm (PDI = 0.04) and a representative TEM image confirmed a spherical morphology (see Figure S2 in the Supporting Information). A 15% w/w dispersion of such $PLMA_{194}$–$PHEMA_{2574}$ nanoparticles exhibited a thermal conductivity of 6.0% at 25 °C compared to that of PAO alone. This most likely represents the maximum possible enhancement that is achievable for such formulations while remaining below a sulfur content of 25 ppm.

https://doi.org/10.1021/acsapm.6c03043
ACS Appl. Polym. Mater. XXXX, XXX, XXX–XXX

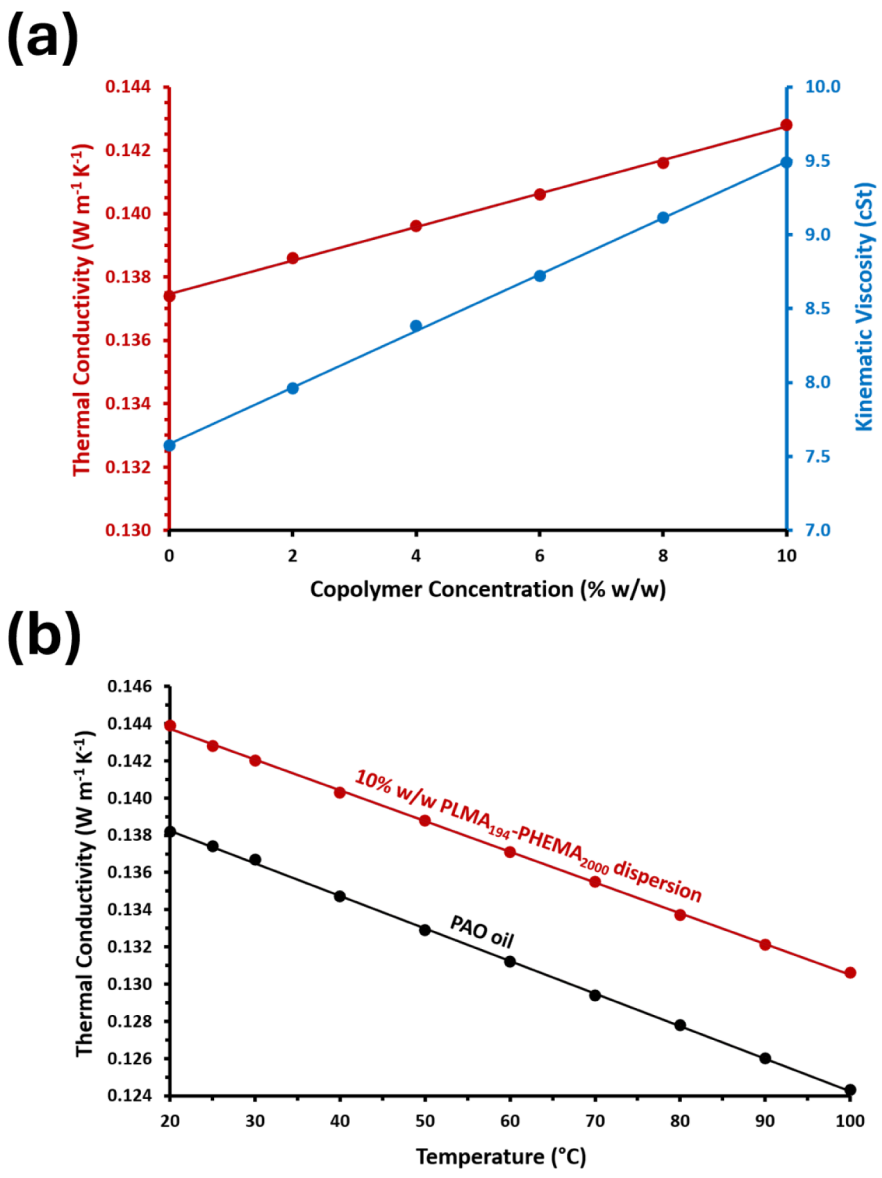

Figure 3. (a) Concentration dependence of the thermal conductivity of a dispersion of $PLMA_{194}$–$PHEMA_{2000}$ nanoparticles in PAO oil at 25 °C and the effect of varying the nanoparticle concentration on kinematic viscosity at 25 °C. (b) Effect of varying the temperature on the thermal conductivity of a 10% w/w dispersion of $PLMA_{194}$–$PHEMA_{2000}$ nanoparticles (thermal conductivity data obtained for the PAO oil alone are included as a reference). [N.B. Error bars for thermal conductivities are smaller than the size of the data points].

A linear reduction in the thermal conductivity of a 10% w/w dispersion of the $PLMA_{194}$–$PHEMA_{2000}$ nanoparticles is observed on heating from 20 to 100 °C (see Figure 3b). Moreover, such thermal conductivities always remain proportionately higher (by 0.0057 W m^{-1} K^{-1} at 20 °C and by 0.0063 W m^{-1} K^{-1} at 100 °C) than those obtained for the PAO oil alone. This is not unexpected: similar data have been reported for various oil-dispersible nanoparticles in the literature.[42] $PLMA_{194}$–$PHEMA_{2000}$ nanoparticles prepared at 20% w/w solids were also examined at 30 °C and 100 kHz as a function of nanoparticle concentration. Dielectric constants of 2.14, 2.23, and 2.32 were determined for 5%, 10% and 15% w/w $PLMA_{194}$–$PHEMA_{2000}$ nanoparticle dispersions, compared to a value of 2.07 for the base oil alone. These observations indicate that the highly polar PHEMA cores have minimal effect on the dielectric properties of such nanoparticle dispersions.

Characterization of Acid-Swollen $PLMA_{194}$–$PHEMA_{2000}$ Nanoparticles

It is well-known that PHEMA can be swollen with water without undergoing dissolution.[43,44] Thus, we decided to examine whether the PHEMA cores of these $PLMA_{194}$–$PHEMA_{2000}$ nanoparticles could be swollen with water to enhance the thermal conductivity of such dispersions. Initial experiments confirmed successful water uptake but the swollen nanoparticles became colloidally unstable on standing within 1 week. However, much better results were obtained if water was replaced with an aqueous solution of 0.30 M HCl (see Figure 4a). DLS studies confirmed that the nanoparticle cores could be swollen with up to 30% w/w aqueous HCl (based on the PHEMA mass) without any loss of colloidal stability while retaining the relatively narrow particle size distribution exhibited by the as-prepared (non-swollen) nanoparticles (DLS polydispersities always remained below 0.03). Attempted swelling of the same nanoparticles with either 40 or 50% w/w

https://doi.org/10.1021/acsapm.6c03043
ACS Appl. Polym. Mater. XXXX, XXX, XXX−XXX

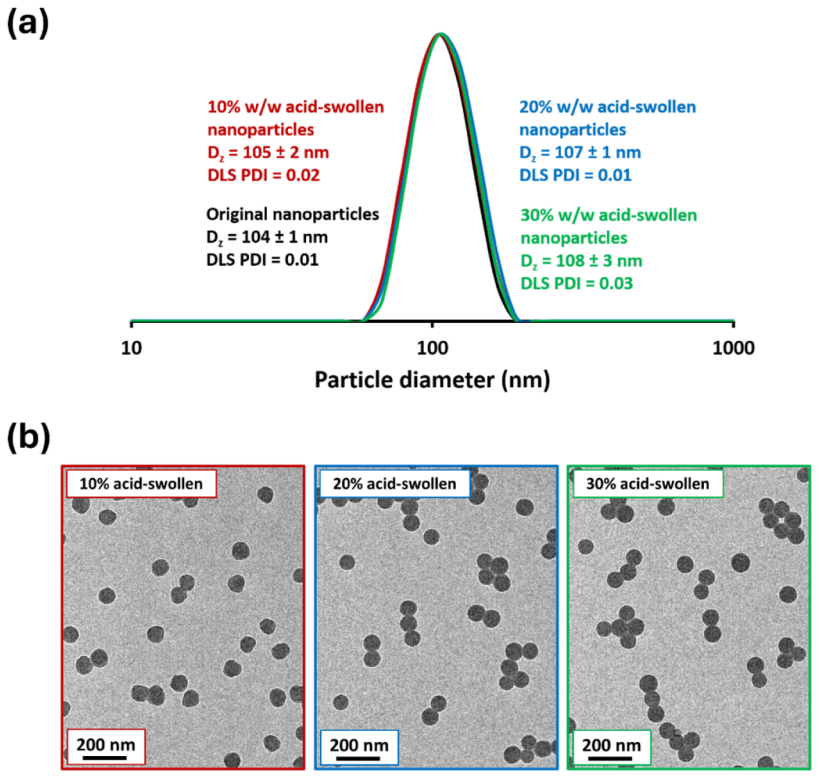

Figure 4. (a) DLS particle size distributions recorded for 0.1% w/w dispersions of the 10, 20 and 30% w/w acid-swollen nanoparticles plus the original unswollen nanoparticles. (b) Representative TEM images recorded for these acid-swollen nanoparticle dispersions.

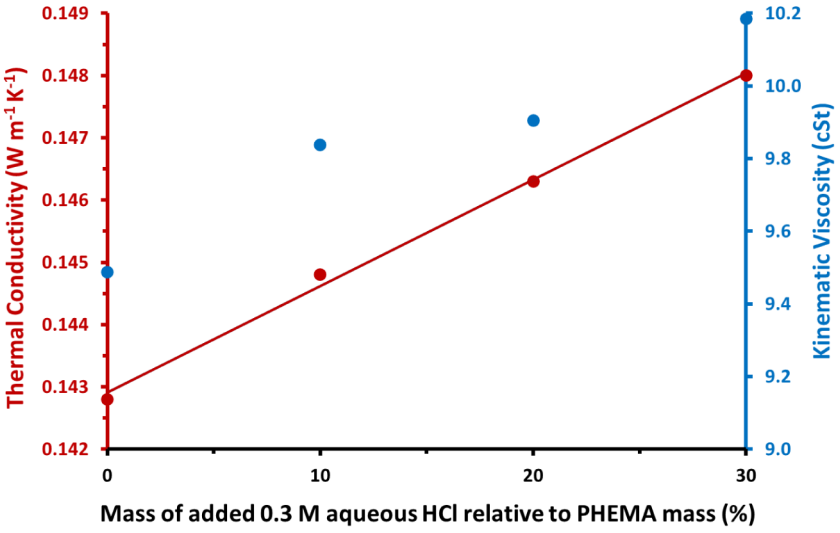

Figure 5. Effect of swelling the PHEMA cores of $PLMA_{194}$–$PHEMA_{2000}$ nanoparticles using increasing amounts of aqueous HCl on the thermal conductivity of a 10% w/w dispersion at 25 °C and the effect on the kinematic viscosity of such acid-swollen nanoparticle dispersions at 25 °C. [N.B. Error bars for thermal conductivities are smaller than the size of the data points].

aqueous HCl led to colloidally unstable nanoparticles as judged by visual inspection. Moreover, drying such acid-swollen nanoparticles under high vacuum prior to TEM studies led to a distinctly more spherical morphology compared to that for the original nanoparticles (see Figure 4b).

Importantly, the thermal conductivity of these acid-swollen nanoparticles at 25 °C increased linearly with their aqueous acid content and was significantly higher than that of the as-prepared (nonswollen) nanoparticles (see Figure 5). Moreover, the corresponding increase in the kinematic viscosity was monotonic but nonlinear.

Characterization of the Silica-Loaded $PLMA_{194}$–$PHEMA_{2000}$ Nanoparticles

In principle, it should be feasible to use the acid-swollen nanoparticles described above as nanoreactors for the *in situ* growth of various inorganic oxides such as silica, titania or alumina.[45−57] This provides a potentially useful means of enhancing the thermal conductivity of such nanoparticle dispersions. For example, the thermal conductivity of silica is

https://doi.org/10.1021/acsapm.6c03043
ACS Appl. Polym. Mater. XXXX, XXX, XXX−XXX

~1.4 W m^{-1} K^{-1}, which is significantly higher than that of either water (0.60 W m^{-1} K^{-1}) or oil (typically 0.13 W m^{-1} K^{-1}).[7,8,58] Accordingly, we examined the *in situ* synthesis of silica within nanoparticle cores using tetraethyl orthosilicate (TEOS) as an oil-soluble precursor (see Scheme 1). Such sol–gel chemistry is expected to lead to extensive cross-linking of the nanoparticle cores owing to participation of the primary hydroxy groups on the PHEMA chains. Two syntheses were conducted in which the water/TEOS molar ratio was either 4.0 or 2.2, with the latter value corresponding to a higher target silica loading by mass (see Figure S5). In each case, DLS studies of the resulting silica-loaded nanoparticles confirmed retention of colloidal stability, with only a modest increase in the hydrodynamic z-average nanoparticle diameter (see Figure 6a) compared to that of the as-prepared original nanoparticles (see Figure 4a). This is in striking contrast to the silica nanofluids prepared by Timofeeva et al., who observed the formation of aggregates when using ultrasonics to disperse 15 nm silica nanoparticles in a synthetic oil (Therminol 66) in the presence of a cationic surfactant.[11] TEM studies indicated that the original spherical morphology is retained for the silica-loaded nanoparticles but with no discernible evidence of the silica component within the nanoparticle cores. However, silicon X-ray mapping experiments conducted for the 26.7% silica-loaded $PLMA_{194}$–$PHEMA_{2000}$ nanoparticles and the precursor $PLMA_{194}$–$PHEMA_{2000}$ nanoparticles are more informative, see Figure S6. These images confirm that the silica produced via acid hydrolysis of the TEOS precursor is indeed formed within the nanoparticle cores, as expected. Thermogravimetric analysis of the dried silica-loaded nanoparticles indicated a silica mass loading of either 17.6% (water/TEOS molar ratio = 4.0) or 26.7% (water/TEOS molar ratio = 2.2). Notably, the as-prepared $PLMA_{194}$–$PHEMA_{2000}$ nanoparticles underwent complete combustion when analyzed under the same conditions, which confirmed that the incombustible residue obtained at 600 °C corresponded entirely to the refractory silica component (see Figure 6c).[59]

Solution densitometry measurements of the original $PLMA_{194}$–$PHEMA_{2000}$ nanoparticles indicated a density of 1.18 g cm^{-3} for the as-synthesized nanoparticles, which increased to either 1.36 g cm^{-3} or 1.50 g cm^{-3} for nanoparticles with silica loadings of 17.6% or 26.7% w/w, respectively (Figure S7). The original $PLMA_{194}$–$PHEMA_{2000}$ nanoparticles, the acid-swollen nanoparticles and the silica-loaded nanoparticles (26.7% w/w silica) were analyzed by SAXS. The corresponding $I(q)$ vs q plots are shown in Figure 6b. Multiple intensity minima associated with the particle form factor are observed, which indicates the formation of well-defined, near-monodisperse nanoparticles in each case. The low q gradient is essentially zero in each case, which implies that the spherical morphology of the original nanoparticles is retained after acid swelling and *in situ* silicification. The corona block makes a relatively small contribution to the overall scattering intensity, thus the primary minimum for each pattern approximately corresponds to the volume-average core radius according to the relation $R = 4.49/q_{min}$, where R is the mean nanoparticle radius and q_{min} is the q value for the primary minimum. Thus, we calculate that acid swelling leads to an increase in the nanoparticle core diameter from 75 to 82 nm, which is consistent with uptake of all of the aqueous acid within the PHEMA cores. A further increase in the nanoparticle core diameter to 89 nm is observed after loading with 26.7% w/w silica relative to the mass of copolymer. This

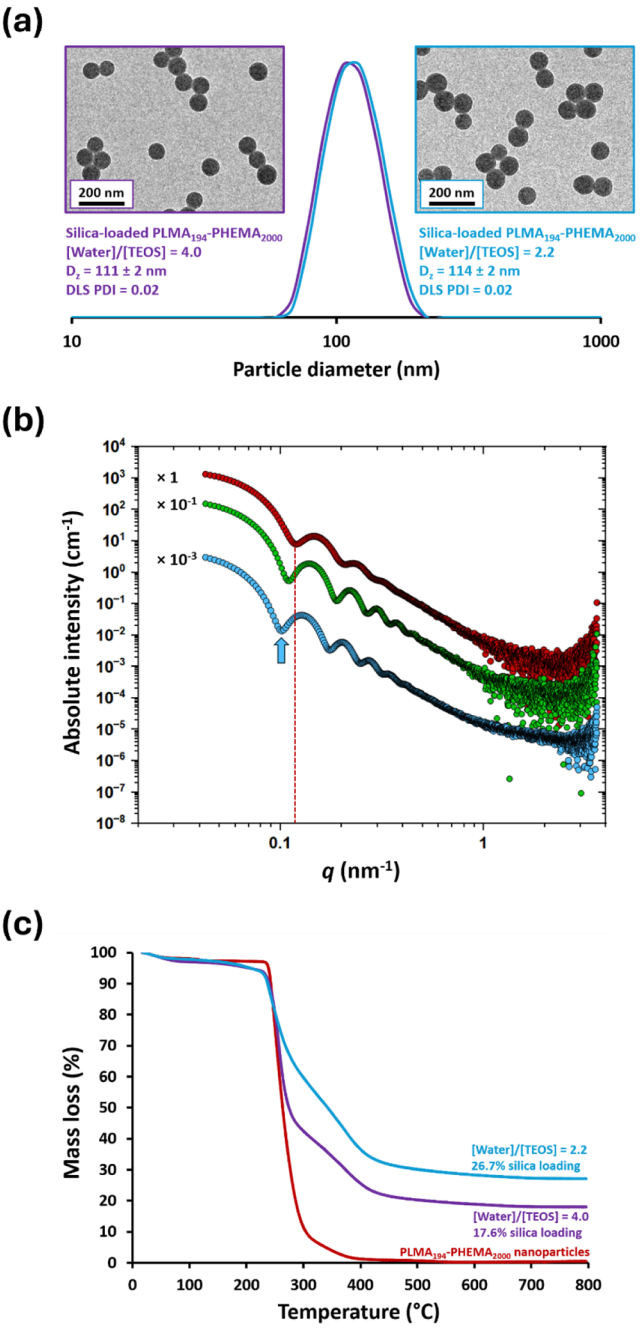

Figure 6. (a) DLS particle size distributions recorded for the silica-loaded $PLMA_{194}$–$PHEMA_{2000}$ nanoparticles prepared using a [water]/[TEOS] molar ratio of either 4.0 or 2.2 (inset: TEM images recorded for these two nanoparticle dispersions). (b) Offset SAXS patterns recorded for a 1.0% w/w PAO dispersion of the as-synthesized $PLMA_{194}$–$PHEMA_{2000}$ nanoparticles (red curve), the aqueous acid-swollen nanoparticles (30% w/w aqueous solution of 0.30 M HCl based on the PHEMA mass; green curve), and the silica-loaded nanoparticles (26.7% silica based on the copolymer mass; blue curve). (c) Thermogravimetry curves recorded in air for the original nanoparticles and the corresponding two examples of silica-loaded nanoparticles.

corresponds to a 28% increase in the core volume compared to that for the acid-swollen nanoparticles and a 67% increase in the core volume compared to that for the as-synthesized nanoparticles. These data are both consistent with and complementary to the DLS data shown in Figure 6a, since

https://doi.org/10.1021/acsapm.6c03043
ACS Appl. Polym. Mater. XXXX, XXX, XXX–XXX

the latter technique reports the overall hydrodynamic z-average diameter (rather than the volume-average core diameter). The SAXS patterns shown in Figure 6b are replotted without any offset parameters in Figure S8. Inspecting the pattern recorded for the silica-loaded nanoparticles (blue data set), it is evident that more intense scattering is obtained at both low and high q.

In the former regime, this reflects the larger final particle size and higher average X-ray scattering contrast compared to that of the original nanoparticles or the aqueous acid-swollen nanoparticles. In the latter regime, this indicates higher X-ray scattering contrast at short length scales, which is consistent with the formation of very small silica blobs within the nanoparticle cores.

In principle, the scattering patterns recorded for the original $PLMA_{194}$–$PHEMA_{2000}$ nanoparticles and the corresponding acid-swollen nanoparticles can be fitted using a well-known spherical micelle model,[60] whereas fitting the pattern obtained for the silica-loaded nanoparticles requires a modified version of the blob model.[61] In practice, such analysis is beyond the scope of the current study.

Highly Transparent Nanoparticle Dispersions

Transmittance vs temperature plots for 11–12% w/w dispersions of silica-loaded $PLMA_{194}$–$PHEMA_{2000}$ nanoparticles in PAO are shown in Figure 7. For nanoparticles containing 17.6% silica, a maximum transmittance (λ = 400 nm) of 95% is observed at around 20 °C, with greater turbidity being discernible at higher temperatures (see inset photograph). In contrast, a similar maximum transmittance is observed at approximately 40 °C for nanoparticles containing 26.7% silica. Thus the silica loading can be used to tune the precise temperature at which highly transparent nanoparticle dispersions are obtained. This is potentially important in the context of thermal management fluids for data centers, where a highly transparent dispersion would enable visual inspection of electrical circuitry for signs of corrosion or malfunctioning components.

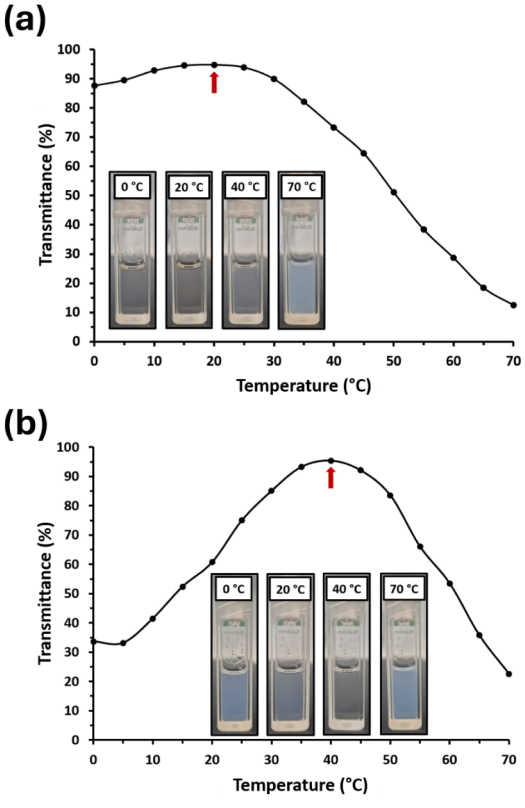

Figure 7. (a) Transmittance (%) vs temperature turbidimetry plots recorded at λ = 400 nm for (a) an 11% w/w dispersion of $PLMA_{194}$–$PHEMA_{2000}$ nanoparticles loaded with 17.6% silica by mass and (b) a 12% w/w dispersion of $PLMA_{194}$–$PHEMA_{2000}$ nanoparticles loaded with 26.7% silica by mass. Inset: Digital photographs recorded for these two nanoparticle dispersions in PAO at 0 °C, 20 °C, 40 and 70 °C.

Thermal Conductivity Studies on Silica-Loaded Nanoparticle Dispersions

The thermal conductivity of the $PLMA_{194}$–$PHEMA_{2000}$ nanoparticles containing 26.7% silica was 0.149 W m^{-1} K^{-1}, which is 8.5% higher than that of the PAO oil alone. For comparison, Zawawi et al. reported a 4.4% increase in thermal conductivity at 303 K (and a corresponding 8.7% increase in dispersion viscosity) for a 0.50% silica nanofluid prepared by dispersing 30 nm silica nanoparticles in PAO.[62] In this case, the nanoparticles were simply dispersed within the PAO without using any polymer or surfactant.

The 26.7% silica-loaded $PLMA_{194}$–$PHEMA_{2000}$ nanoparticles exhibited the expected linear reduction in thermal conductivity up to 70 °C (see Figure 8) but anomalous data were obtained at higher temperatures (data not shown). This was belatedly shown to be due to evaporative loss of the ethanol by-product generated during *in situ* silicification. Thus, each silica-loaded nanoparticle dispersion was heated in turn to 95 °C for 2 h to remove ethanol and water. In both cases, such annealing led to a significant loss in thermal conductivity at any given temperature from 20 to 100 °C (see Figure 8 and Table S3). Nevertheless, thermal conductivities always remained higher than those recorded for the as-prepared $PLMA_{194}$–$PHEMA_{2000}$ nanoparticles and the nanoparticles containing the higher silica mass loading of 26.7% exhibited the highest thermal conductivity. Hence these proof-of-concept experiments demonstrate that the *in situ* formation of a suitable inorganic oxide phase within such nanoparticle cores can be used to enhance the thermal conductivity without any loss of colloidal stability. In future studies, it would be interesting to examine the synthesis of alternative inorganic oxides that offer higher thermal conductivities than silica.[63–70] In this context, the introduction of alumina is likely to be of particular interest.[64–66,68] Unfortunately, this is beyond the scope of the current study.

Colloidal Stability of $PLMA_{194}$–$PHEMA_{2000}$ Nanoparticle Dispersions

A commercially viable thermal management fluid must exhibit excellent colloidal stability when exposed to elevated temperatures, as well as during long-term storage at ambient temperature. DLS studies confirmed that both a 10% w/w dispersion of the $PLMA_{194}$–$PHEMA_{2000}$ nanoparticles and a 12% w/w dispersion of the 26.7% silica-loaded nanoparticles remained colloidally stable after storage for 6 months at 25 °C (see Table S5 and Figure S9 in the Supporting Information). Moreover, the hydrodynamic z-average diameter reported by DLS was essentially unchanged when heating such dispersions from 20 to 80 °C, indicating good thermal stability under such conditions (see Figure S10). [N.B. In such studies, nanoparticle dispersions originally prepared in PAO were diluted fifty-fold using *n*-dodecane prior to DLS analysis simply

https://doi.org/10.1021/acsapm.6c03043
ACS Appl. Polym. Mater. XXXX, XXX, XXX–XXX

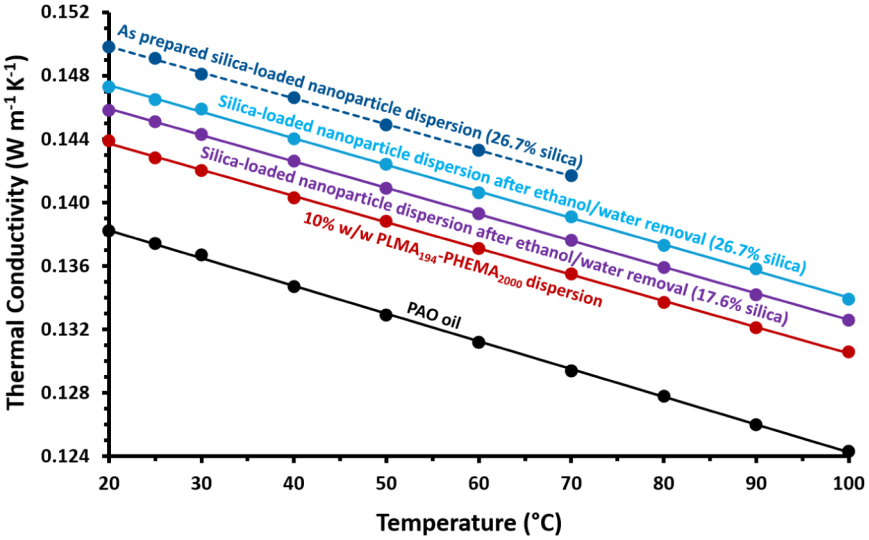

Figure 8. Effect of temperature on the thermal conductivity of the silica-loaded nanoparticle dispersions in comparison to the original $PLMA_{194}$–$PHEMA_{2000}$ dispersion and the PAO oil alone. The dashed line denotes the thermal conductivity data obtained for the as-prepared silica-loaded nanoparticle dispersion (which contain ethanol and water as by-products) and the solid lines (purple and blue data) denote the thermal conductivity data obtained after heating the silica-loaded nanoparticle dispersions at 95 °C for 2 h to remove ethanol and water. [N.B. Error bars for thermal conductivities are smaller than the size of the data points].

because the refractive index and viscosity of the latter solvent are known over a wide temperature range].

CONCLUSIONS

Diblock copolymer nanoparticles with polar cores can be conveniently prepared directly in a poly(α-olefin) oil via RAFT dispersion polymerization. This PISA formulation enables well-defined spherical nanoparticles of around 100 nm diameter to be prepared at up to 30% w/w solids with excellent long-term colloidal stability and relatively low dispersion viscosity. Despite the use of RAFT polymerization, such dispersions can have an overall sulfur content below 25 ppm provided that a dithiobenzoate-based chain transfer agent is used to target a relatively long core-forming PHEMA block. Under such conditions, the thermal conductivity can be boosted by up to 6.0% relative to that of the poly(α-olefin) oil alone. The polar PHEMA cores of these nanoparticles can be swollen with aqueous acid, which further enhances the thermal conductivity compared to that of the base oil. Moreover, such acid-swollen nanoparticles can act as nanoreactors when using an oil-soluble tetraethyl orthosilicate (TEOS) precursor for the *in situ* synthesis of silica within their cores without loss of colloidal stability. The resulting silica-loaded nanoparticles result in an increase in thermal conductivity of up to 8.5% at 25 °C. Moreover, varying their silica content enables the temperature at which such nanoparticle dispersions exhibit maximum transparency to be adjusted from 20 to 40 °C. In principle, such nanocomposite nanoparticles offer potential applications as next-generation thermal management fluids for the efficient heat dissipation that is required for data centers and fast-charging batteries.

ASSOCIATED CONTENT

Supporting Information

The Supporting Information is available free of charge at https://pubs.acs.org/doi/10.1021/acsapm.6c03043.

Tabulated summary of reaction conditions for nanoparticle syntheses; DLS data and TEM images for $PLMA_{194}$–$PHEMA_{2000}$ nanoparticle syntheses performed at 10–40% w/w solids; DLS data and TEM image for $PLMA_{194}$–$PHEMA_{2600}$ nanoparticle synthesis at 15% w/w; DLS data and TGA curves obtained for a series of silica-loaded nanoparticles; solution mass densities and SAXS curves of as-prepared, acid-swollen and silica-loaded $PLMA_{194}$–$PHEMA_{2000}$ nanoparticles; tabulated summary of density, kinematic viscosity and thermal conductivity data recorded at 25 °C; density and kinematic viscosity data measured at 40–70 °C for the PAO oil and 10% w/w $PLMA_{194}$–$PHEMA_{2000}$ nanoparticles; effect of temperature on the kinematic viscosity of PAO oil and 10% w/w $PLMA_{194}$–$PHEMA_{2000}$ nanoparticles; effect of temperature on the dynamic viscosity at different shear rates for PAO oil and 10% w/w $PLMA_{194}$–$PHEMA_{2000}$ nanoparticles; DLS data for selected, freshly prepared and aged nanoparticles; DLS data obtained at 20–80 °C for the $PLMA_{194}$–$PHEMA_{2000}$ nanoparticles and the corresponding silica-loaded nanoparticles (PDF)

AUTHOR INFORMATION

Corresponding Author

Steven P. Armes – *Dainton Building, School of Mathematical and Physical Sciences, University of Sheffield, Sheffield, South Yorkshire S3 7HF, U.K.;* orcid.org/0000-0002-8289-6351; Email: s.p.armes@sheffield.ac.uk

Authors

Priyanka Chohan – *Dainton Building, School of Mathematical and Physical Sciences, University of Sheffield, Sheffield, South Yorkshire S3 7HF, U.K.*

Oleksandr O. Mykhaylyk – *Dainton Building, School of Mathematical and Physical Sciences, University of Sheffield, Sheffield, South Yorkshire S3 7HF, U.K.;* orcid.org/0000-0003-4110-8328

https://doi.org/10.1021/acsapm.6c03043
ACS Appl. Polym. Mater. XXXX, XXX, XXX–XXX

Giles M. Prentice − *Fluid Research, Castrol Technology Centre, Reading RG8 7QR, U.K.*
David J. Atkinson − *Fluid Research, Castrol Technology Centre, Reading RG8 7QR, U.K.*

Complete contact information is available at: https://pubs.acs.org/10.1021/acsapm.6c03043

Notes

The authors declare no competing financial interest.

■ ACKNOWLEDGMENTS

Castrol Ltd. (Pangbourne, UK) is thanked for funding a PhD studentship for the first author and for permission to publish these results. Dr. George Sanderson (GEO Specialty Chemicals, Hythe, UK) is thanked for providing the high-purity HEMA monomer used in this study. The authors thank Dr. Svetomir Tzokov at the University of Sheffield Biomedical Science Electron Microscopy Suite for his assistance with the TEM studies. Dr. Liam Hughes is also thanked for recording TEM-EDX images. Dr. Andi Xie is thanked for his assistance with the SAXS analysis. The ESRF is thanked for beam time on ID02 (beamline proposal SC-5764).

■ REFERENCES

(1) Sohel Murshed, S. M.; Nieto de Castro, C. A. A Critical Review of Traditional and Emerging Techniques and Fluids for Electronics Cooling. *Renewable Sustainable Energy Rev.* **2017**, *78*, 821−833.
(2) Wu, W.; Wang, S.; Wu, W.; Chen, K.; Hong, S.; Lai, Y. A Critical Review of Battery Thermal Performance and Liquid Based Battery Thermal Management. *Energy Convers. Manage* **2019**, *182*, 262−281.
(3) Deng, J.; Bae, C.; Denlinger, A.; Miller, T. Electric Vehicles Batteries: Requirements and Challenges. *Joule* **2020**, *4*, 511−515.
(4) Luo, J.; Zou, D.; Wang, Y.; Wang, S.; Huang, J. Battery Thermal Management Systems (BTMs) Based on Phase Change Material (PCM): A Comprehensive Review. *Chem. Eng. J.* **2022**, *430*, 132741.
(5) Luo, Q.; Wang, C.; Wen, H.; Liu, L. L.-C. I. H. M. undefined.Research and Optimization of Thermophysical Properties of Sic Oil-Based Nanofluids for Data Center Immersion Cooling. *Int. Commun. Heat Mass Transfer.* **2022**, *131*, 105863.
(6) MarketsandMarkets *Thermic Fluid Market by Type (Organic, Inorganic), Application (Chemical, Oil & Gas, Food & Beverages, Solar Power, Pharmaceuticals), and Region (North America, Europe, APAC, RoW) - Global Forecast to 2026*. 2021. https://www.marketsandmarkets.com/Market-Reports/thermic-fluid-market-861.html (Accessed 2026−03−06).
(7) Huber, M. L.; Perkins, R. A.; Friend, D. G.; Sengers, J. V.; Assael, M. J.; Metaxa, I. N.; Miyagawa, K.; Hellmann, R.; Vogel, E. New International Formulation for the Thermal Conductivity of H2O. *J. Phys. Chem. Ref. Data* **2012**, *41*, 033102.
(8) Engineering ToolBox. *Liquids - Thermal Conductivities*. https://www.engineeringtoolbox.com/thermal-conductivity-liquids-d_1260.html (Accessed 2026−03−17).
(9) Keblinski, P.; Eastman, J. A.; Cahill, D. G. Nanofluids for Thermal Transport. *Mater. Today* **2005**, *8*, 36−44.
(10) Choi, C.; Yoo, H. S.; Oh, J. M. Preparation and Heat Transfer Properties of Nanoparticle-in-Transformer Oil Dispersions as Advanced Energy-Efficient Coolants. *Curr. Appl. Phys.* **2008**, *8*, 710−712.
(11) Timofeeva, E. V.; Moravek, M. R.; Singh, D. Improving the Heat Transfer Efficiency of Synthetic Oil with Silica Nanoparticles. *J. Colloid Interface Sci.* **2011**, *364*, 71−79.
(12) Nižetić, S.; Jurčević, M.; Arıcı, M.; Arasu, A. V.; Xie, G. Nano-Enhanced Phase Change Materials and Fluids in Energy Applications: A Review. *Renewable Sustainable Energy Rev.* **2020**, *129*, 109931.
(13) Jadhav, R. M.; Kumar, G.; Balasubramanian, N.; Sangwai, J. S. Synergistic Effect of Nickel Nanoparticles with Tetralin on the Rheology and Upgradation of Extra Heavy Oil. *Fuel* **2022**, *308*, 122035.
(14) Yu, Q.; Song, Y.; Cui, C.; Cao, F. Effects of Nanoparticle Aggregation on the Thermal Conductivity of Nanofluids: A Comprehensive Review Based on Multiscale Methods. *Renewable Sustainable Energy Rev.* **2026**, *226*, 116306.
(15) Houillot, L.; Bui, C.; Farcet, C.; Moire, C.; Raust, J.-A.; Pasch, H.; Save, M.; Charleux, B. Dispersion Polymerization of Methyl Acrylate in Nonpolar Solvent Stabilized by Block Copolymers Formed In Situ via the RAFT Process. *ACS Appl. Mater. Interfaces* **2010**, *2*, 434−442.
(16) Fielding, L. A.; Derry, M. J.; Ladmiral, V.; Rosselgong, J.; Rodrigues, A. M.; Ratcliffe, L. P. D.; Sugihara, S.; Armes, S. P. RAFT Dispersion Polymerization in Non-Polar Solvents: Facile Production of Block Copolymer Spheres, Worms and Vesicles in n-Alkanes. *Chem. Sci.* **2013**, *4*, 2081−2087.
(17) Fielding, L. A.; Lane, J. A.; Derry, M. J.; Mykhaylyk, O. O.; Armes, S. P. Thermo-Responsive Diblock Copolymer Worm Gels in Non-Polar Solvents. *J. Am. Chem. Soc.* **2014**, *136*, 5790−5798.
(18) Pei, Y.; Noy, J. M.; Roth, P. J.; Lowe, A. B. Soft Matter Nanoparticles with Reactive Coronal Pentafluorophenyl Methacrylate Residues via Non-Polar RAFT Dispersion Polymerization and Polymerization-Induced Self-Assembly. *J. Polym. Sci., Part A: Polym. Chem.* **2015**, *53*, 2326−2335.
(19) Derry, M. J.; Fielding, L. A.; Armes, S. P. Industrially-Relevant Polymerization-Induced Self-Assembly Formulations in Non-Polar Solvents: RAFT Dispersion Polymerization of Benzyl Methacrylate. *Polym. Chem.* **2015**, *6*, 3054−3062.
(20) Derry, M. J.; Fielding, L. A.; Warren, N. J.; Mable, C. J.; Smith, A. J.; Mykhaylyk, O. O.; Armes, S. P. In Situ Small-Angle X-Ray Scattering Studies of Sterically-Stabilized Diblock Copolymer Nanoparticles Formed during Polymerization-Induced Self-Assembly in Non-Polar Media. *Chem. Sci.* **2016**, *7*, 5078−5090.
(21) Derry, M. J.; Fielding, L. A.; Armes, S. P. Polymerization-Induced Self-Assembly of Block Copolymer Nanoparticles via RAFT Non-Aqueous Dispersion Polymerization. *Prog. Polym. Sci.* **2016**, *52*, 1−18.
(22) Derry, M. J.; Mykhaylyk, O. O.; Armes, S. P. A Vesicle-to-Worm Transition Provides a New High-Temperature Oil Thickening Mechanism. *Angew. Chem., Int. Ed.* **2017**, *56*, 1746−1750.
(23) Cornel, E. J.; Van Meurs, S.; Smith, T.; O'Hora, P. S.; Armes, S. P. In Situ Spectroscopic Studies of Highly Transparent Nanoparticle Dispersions Enable Assessment of Trithiocarbonate Chain-End Fidelity during RAFT Dispersion Polymerization in Nonpolar Media. *J. Am. Chem. Soc.* **2018**, *140*, 12980−12988.
(24) Derry, M. J.; Smith, T.; O'Hora, P. S.; Armes, S. P. Block Copolymer Nanoparticles Prepared via Polymerization-Induced Self-Assembly Provide Excellent Boundary Lubrication Performance for Next-Generation Ultralow-Viscosity Automotive Engine Oils. *ACS Appl. Mater. Interfaces* **2019**, *11*, 33364−33369.
(25) Parker, B. R.; Derry, M. J.; Ning, Y.; Armes, S. P. Exploring the Upper Size Limit for Sterically Stabilized Diblock Copolymer Nanoparticles Prepared by Polymerization-Induced Self-Assembly in Non-Polar Media. *Langmuir* **2020**, *36*, 3730−3736.
(26) Häkkinen, S.; Tanaka, J.; Garcia Maset, R.; Hall, S. C. L.; Huband, S.; Rho, J. Y.; Song, Q.; Perrier, S. Polymerisation-Induced Self-Assembly of Graft Copolymers. *Angew. Chem., Int. Ed.* **2022**, *61*, No. e202210518.
(27) Gardoni, G.; Manfredini, N.; Monzani, M.; Sponchioni, M.; Moscatelli, D. Thermoresponsive Modular Nano-Objects Via RAFT Dispersion Polymerization in a Non-Polar Solvent. *ACS Appl. Polym. Mater.* **2023**, *5*, 494−503.
(28) Gardoni, G.; Manfredini, N.; Bagnato, G.; Sponchioni, M.; Moscatelli, D. Role of the Polymer Microstructure in Controlling Colloidal and Thermo-Responsive Properties of Nano-Objects Prepared Via RAFT Polymerization in a Non-Polar Medium. *Langmuir* **2023**, *39*, 10133−10144.
(29) György, C.; Kirkman, P. M.; Neal, T. J.; Chan, D. H. H.; Williams, M.; Smith, T.; Growney, D. J.; Armes, S. P. Enhanced

Adsorption of Epoxy-Functional Nanoparticles onto Stainless Steel Significantly Reduces Friction in Tribological Studies. *Angew. Chem., Int. Ed.* **2023**, *62*, No. e202218397.
(30) György, C.; Armes, S. P. Recent Advances in Polymerization-Induced Self-Assembly (PISA) Syntheses in Non-Polar Media. *Angew. Chem., Int. Ed.* **2023**, *62*, No. e202308372.
(31) Cunningham, V. J.; Armes, S. P.; Musa, O. M. S. Characterisation and Pickering Emulsifier Performance of Poly(Stearyl Methacrylate)−Poly(N-2-(Methacryloyloxy)Ethyl Pyrrolidone) Diblock Copolymer Nano-Objects via RAFT Dispersion Polymerisation in n-Dodecane. *Polym. Chem.* **2016**, *7*, 1882−1891.
(32) Chohan, P.; György, C.; Mykhaylyk, O. O.; Prentice, G. M.; Filip, S. V.; Payne, M. J.; Manna, G.; Armes, S. P. RAFT Dispersion Polymerization of 2-Hydroxyethyl Methacrylate in Non-Polar Media. *Macromolecules* **2024**, *57*, 11738−11752.
(33) Chiefari, J.; Chong, Y. K.; Ercole, F.; Krstina, J.; Jeffery, J.; Le, T. P. T.; Mayadunne, R. T. A.; Meijs, G. F.; Moad, C. L.; Moad, G.; Rizzardo, E.; Thang, S. H. Living Free-Radical Polymerization by Reversible Addition-Fragmentation Chain Transfer: The RAFT Process. *Macromolecules* **1998**, *31*, 5559−5562.
(34) Moad, G.; Rizzardo, E.; Thang, S. H. Living Radical Polymerization by the RAFT Process. *Aust. J. Chem.* **2005**, *58* (6), 379−410.
(35) Yang, P.; Lu, X.; Huang, P.; Wu, K.; Shi, J. High Thermal Conductivity Polymer Blend Films with Excellent Mechanical and Recyclable Properties Based on Hydrogen Bonding Interactions. *ACS Appl. Polym. Mater.* **2026**, *8*, 6659.
(36) Trent, J. S. Ruthenium Tetraoxide Staining of Polymers: New Preparative Methods for Electron Microscopy. *Macromolecules* **1984**, *17*, 2930−2931.
(37) Chèvremont, W.; Narayanan, T. A Correction Procedure for Secondary Scattering Contributions from Windows in Small-Angle X-Ray Scattering and Ultra-Small-Angle X-Ray Scattering. *J. Appl. Crystallogr.* **2024**, *57*, 440−445.
(38) Ilavsky, J.; Jemian, P. Irena: tool suite for modeling and analysis of small-angle scattering. *J. Appl. Crystallogr.* **2009**, *42*, 347−353.
(39) Shi, Q.; Wu, J. Review on Sulfur Compounds in Petroleum and Its Products: State-of-the-Art and Perspectives. *Energy Fuels* **2021**, *35*, 14445−14461.
(40) Bannister, I.; Billingham, N. C.; Armes, S. P.; Rannard, S. P.; Findlay, P. Development of Branching in Living Radical Copolymerization of Vinyl and Divinyl Monomers. *Macromolecules* **2006**, *39*, 7483−7492.
(41) Rosselgong, J.; Armes, S. P.; Barton, W.; Price, D. Synthesis of Highly Branched Methacrylic Copolymers: Observation of Near-Ideal Behavior Using RAFT Polymerization. *Macromolecules* **2009**, *42*, 5919−5924.
(42) Du, B. Investigating the Influence of Different Types of Nanoparticles on Thermal and Dielectric Properties of Insulation in Converter Transformer. In *Properties and Applications of Polymer Dielectrics*; IntechOpen, 2017.
(43) Ramaraj, B.; Radhakrishnan, G. Modification of the Dynamic Swelling Behaviour of Poly(2-Hydroxyethyl Methacrylate) Hydrogels in Water through Interpenetrating Polymer Networks (IPNs). *Polymer.* **1994**, *35*, 2167−2173.
(44) Wang, L.; Lu, C.; Liu, H.; Lin, S.; Nan, K.; Chen, H.; Li, L. A Double Network Strategy to Improve Epithelization of a Poly(2-Hydroxyethyl Methacrylate) Hydrogel for Corneal Repair Application. *RSC Adv.* **2016**, *6*, 1194−1202.
(45) Hench, L. L.; West, J. K. The Sol-Gel Process. *Chem. Rev.* **1990**, *90*, 33−72.
(46) Bronstein, L. M.; Sidorov, S. N.; Valetsky, P. M.; Hartmann, J.; Cölfen, H.; Antonietti, M. Induced Micellization by Interaction of Poly(2-Vinylpyridine)-Block-Poly(Ethylene Oxide) with Metal Compounds. Micelle Characteristics and Metal Nanoparticle Formation. *Langmuir* **1999**, *15*, 6256−6262.
(47) Liu, S.; Weaver, J. V. M.; Save, M.; Armes, S. P. Synthesis of PH-Responsive Shell Cross-Linked Micelles and Their Use as Nanoreactors for the Preparation of Gold Nanoparticles. *Langmuir* **2002**, *18*, 8350−8357.
(48) Pileni, M. P. The Role of Soft Colloidal Templates in Controlling the Size and Shape of Inorganic Nanocrystals. *Nat. Mater.* **2003**, *2*, 145−150.
(49) Lu, Y.; Mei, Y.; Drechsler, M.; Ballauff, M. Thermosensitive Core-Shell Particles as Carriers for Ag Nanoparticles: Modulating the Catalytic Activity by a Phase Transition in Networks. *Angew. Chem., Int. Ed.* **2006**, *45*, 813−816.
(50) Huo, Q.; Liu, J.; Wang, L.-Q.; Jiang, Y.; Lambert, T. N.; Fang, E. A New Class of Silica Cross-Linked Micellar Core-Shell Nanoparticles. *J. Am. Chem. Soc.* **2006**, *128*, 6447−6453.
(51) Khanal, A.; Inoue, Y.; Yada, M.; Nakashima, K. Synthesis of Silica Hollow Nanoparticles Templated by Polymeric Micelle with Core−Shell−Corona Structure. *J. Am. Chem. Soc.* **2007**, *129*, 1534−1535.
(52) Yuan, J. J.; Mykhaylyk, O. O.; Ryan, A. J.; Armes, S. P. Cross-Linking of Cationic Block Copolymer Micelles by Silica Deposition. *J. Am. Chem. Soc.* **2007**, *129*, 1717−1723.
(53) Kim, K. T.; Cornelissen, J. J. L. M.; Nolte, R. J. M.; Van Hest, J. C. M. A Polymersome Nanoreactor with Controllable Permeability Induced by Stimuli-Responsive Block Copolymers. *Adv. Mater.* **2009**, *21*, 2787−2791.
(54) Jing, J.; Feng, J.; Li, W.; Yu, W. W. Low-Temperature Synthesis of Water-Dispersible Anatase Titanium Dioxide Nanoparticles for Photocatalysis. *J. Colloid Interface Sci.* **2013**, *396*, 90−94.
(55) Singh, L. P.; Bhattacharyya, S. K.; Kumar, R.; Mishra, G.; Sharma, U.; Singh, G.; Ahalawat, S. Sol-Gel Processing of Silica Nanoparticles and Their Applications. *Adv. Colloid Interface Sci.* **2014**, *214*, 17−37.
(56) Peters, R. J. R. W.; Marguet, M.; Marais, S.; Fraaije, M. W.; Van Hest, J. C. M.; Lecommandoux, S. Cascade Reactions in Multicompartmentalized Polymersomes. *Angew. Chem., Int. Ed.* **2014**, *53*, 146−150.
(57) Swisher, J. H.; Jibril, L.; Petrosko, S. H.; Mirkin, C. A. Nanoreactors for Particle Synthesis. *Nat. Rev. Mater.* **2022**, *7*, 428−448.
(58) Grove, A. S. *Physics and Technology of Semiconductor Devices*; John Wiley & Sons, 1967.
(59) Göktaş, M.; Aykaç, C.; Akinay, Y. Synthesis and Characterization of Block Copolymer: Thermal and Morphological Properties of SiO2-Filled Block Copolymer Nanocomposites. *Polym. Bull* **2023**, *80*, 8565−8584.
(60) Pedersen, J. S. Form Factors of Block Copolymer Micelles with Spherical, Ellipsoidal and Cylindrical Cores. *J. Appl. Crystallogr.* **2000**, *33*, 637−640.
(61) Pedersen, J. S.; Hamley, I. W.; Ryu, C. Y.; Lodge, T. P. Contrast Variation Small-Angle Neutron Scattering Study of the Structure of Block Copolymer Micelles in a Slightly Selective Solvent at Semidilute Concentrations. *Macromolecules* **2000**, *33*, 542−550.
(62) Zawawi, N. N. M.; Azmi, W. H.; Aminullah, A. R. M.; Ali, H. M. Polyalphaolefin-Based SiO2 Nanolubricants: Thermo-Physical and Tribology Investigations for Electric Vehicle Air-Conditioning System. *Int. J. Refrig* **2025**, *178*, 203−214.
(63) Xie, H.; Yu, W.; Chen, W. MgO Nanofluids: Higher Thermal Conductivity and Lower Viscosity among Ethylene Glycol-Based Nanofluids Containing Oxide Nanoparticles. *J. Exp. Nanosci.* **2010**, *5*, 463−472.
(64) Sridhara, V.; Satapathy, L. N. Al2O3-Based Nanofluids: A Review. *Nanoscale Res. Lett.* **2011**, *6*, 456.
(65) Senthilraja, S.; Vijayakumar, K.; Gangadevi, R. A Comparative Study on Thermal Conductivity of Al2O3/Water, CuO/Water and Al2O3 − CuO/Water Nanofluids. *Dig. J. Nanomater. Biostruct* **2015**, *10*, 1449.
(66) Iqbal, S. M.; Raj, C. S.; Michael, J. J.; Irfan, A. M. A Comparative Investigation of Al2O3/H2O, SiO2/H2O and ZrO2/H2O Nanofluid for Heat Transfer Applications. *Dig. J. Nanomater. Biostruct* **2017**, *12*, 255−263.

(67) Simpson, S.; Schelfhout, A.; Golden, C.; Vafaei, S. Nanofluid Thermal Conductivity and Effective Parameters. *Appl. Sci.* **2019**, *9*, 87−142.
(68) Xiang, D.; Shen, L.; Wang, H. Investigation on the Thermal Conductivity of Mineral Oil-Based Alumina/Aluminum Nitride Nanofluids. *Materials* **2019**, *12*, 4217.
(69) Younes, H.; Mao, M.; Sohel Murshed, S. M.; Lou, D.; Hong, H.; Peterson, G. P. Nanofluids: Key Parameters to Enhance Thermal Conductivity and Its Applications. *Appl. Therm. Eng.* **2022**, *207*, 118202.
(70) Galpaya, G. D. C. P.; Gunasena, M. D. K. M.; Induranga, D. K. A.; Priyadarshana, H. V. V.; Indupama, S. V. A. A.; Wijesekara, E. R. J. M. D. D. P.; Ishra, M. I.; Mantilaka, M. M. M. G. P. G.; Koswattage, K. R. Nanoparticle-Enhanced Engine Oils for Automotive Applications: Thermal Conductivity and Heat Capacity Improvements. *Molecules* **2025**, *30*, 2695.

https://doi.org/10.1021/acsapm.6c03043
ACS Appl. Polym. Mater. XXXX, XXX, XXX−XXX